෴

# Controlling the effective mass of quantum well states in Pb/Si(111) by interface engineering

Bartosz Slomski,[1,2,*] Fabian Meier,[1,2] Jürg Osterwalder,[1] and J. Hugo Dil[1,2]

[1]*Physik-Institut, Universität Zürich, Winterthurerstrasse 190, CH-8057 Zürich, Switzerland*
[2]*Swiss Light Source, Paul Scherrer Institut, CH-5232 Villigen, Switzerland*

The in-plane effective mass of quantum well states in thin Pb films on a Bi reconstructed Si(111) surface is studied by angle-resolved photoemission spectroscopy. It is found that this effective mass is a factor of 3 lower than the unusually high values reported for Pb films grown on a Pb reconstructed Si(111) surface. Through a quantitative low-energy electron diffraction analysis the change in effective mass as a function of coverage and for the different interfaces is linked to a change of about 2% in the in-plane lattice constant. To corroborate this correlation, density functional theory calculations are performed on freestanding Pb slabs with different in-plane lattice constants. These calculations show an anomalous dependence of the effective mass on the lattice constant including a change of sign for values close to the lattice constant of Si(111). This unexpected relation is due to a combination of reduced orbital overlap of the $6p_z$ states and altered hybridization between the $6p_z$ and the $6p_{xy}$ derived quantum well states. Furthermore, it is shown by core-level spectroscopy that the Pb films are structurally and temporally stable at temperatures below 100 K.

## I. INTRODUCTION

The electronic structure of crystalline thin metal films is often dominated by the formation of standing electron waves in the direction perpendicular to the surface. The basic physics behind these quantum well states (QWSs) is well understood[1] and it has been found that a variety of properties follows the predicted dependence on the exact thickness of these films.[2] The growth conditions can depend significantly on the substrate crystal orientation[3] and on the interface reconstruction.[4] Furthermore, the energies of the confined states can be altered via changing the atomic species at the interface.[5] In this work we extend this research and show that also the band dispersion of quantum well states can be altered by interface engineering, exemplified by the system of ultrathin Pb films on Si(111).

The structural and electronic properties of Pb on Si(111) have been studied for almost 30 years. The initial interest focused on the contact between a superconductor (Pb) and a semiconductor (Si). However, the rich variety of unexpected phenomena that were observed has incited research also in temperature ranges far above the superconduction transition temperature $T_C$ of Pb. Examples of these observations are the strong dependence of the Schottky barrier on the exact atomic structure,[6] the formation of magic height islands,[7] anomalies in the superconductivity transition temperature,[8–10] oscillations of the work function, and extremely long excited-state lifetimes,[11,12] and the observation of a Rashba-type spin splitting.[13] The origin of many of these phenomena lies in the peculiar electronic structure of Pb on Si(111) manifested in the high in-plane effective mass.[14–16] Control of this effective mass can thus also lead to control over many of the other physical properties that make Pb films on Si such a rich research subject.

## II. EXPERIMENT

Angle-resolved photoemission spectroscopy (ARPES) and low-energy electron diffraction (LEED) experiments were performed with the COPHEE setup at the Swiss Light Source of the Paul-Scherrer-Institut at the Surface and Interface Beamline. The energy and angular resolution of the spectrometer were set to 30 meV and 0.5°, respectively.[17] In the current experiment the spin resolution was not used. All valence band photoemission data were recorded at a photon energy of 24 eV and the core-level data at 70 eV using horizontally polarized light. The base pressure of the chamber was below $2 \times 10^{-10}$ mbar and the sample temperature during the measurements was $T < 70$ K. An $n$-type Si(111) (44–62 $\Omega$ cm) sample was degassed at 600 K for 24 h and flashed several times above 1300 K to remove adsorbates and to form the $(7 \times 7)$ surface reconstruction. The cleanliness of the sample was checked with ARPES, where the surface states $S1$ and $S2$ at binding energies $E_B = 0.20$ and $0.82$ eV could be identified, as shown in Figs. 1(a) and 1(c). The LEED pattern displayed in Fig. 1(d) confirms the $(7 \times 7)$ surface reconstruction showing intense superstructure spots.

Bi and Pb interfaces were prepared through the deposition of approximately 3 monolayers (ML) of Bi or Pb from a water-cooled Knudsen cell onto the clean Si(111)-$(7 \times 7)$ surface at low temperature and subsequent annealing until the $(\sqrt{3} \times \sqrt{3})$ R30° (henceforth $\sqrt{3}$) surface reconstruction appeared in LEED as shown in Fig. 1(e). From previous studies it is known that Bi has two $\sqrt{3}$ superlattice phases on Si(111) that form depending on the initial coverage and the annealing process.[18] The $\alpha$ phase forms at $T > 640$ K with $\frac{1}{3}$-ML coverage in substrate units (1 ML = $7.83 \times 10^{14}$ atoms/cm$^2$), whereas the denser $\beta$ phase forms for temperatures below 640 K and has a coverage of 1 ML. In our experiment the annealing temperature was around 600 K, hence we conclude that the $\beta$ phase is formed. After creation of this phase the surface states disappear and the top of the valence band (VB) of Si is shifted by 0.35 eV to a lower binding energy, from 2.1 eV initially to 1.75 eV, which is apparent from a comparison of Figs. 1(a) and 1(b). This band shifting indicates that a dipole layer is created.

The Pb $\sqrt{3}$ interface was formed under similar conditions, yielding the $\frac{4}{3}$-ML $\alpha$ phase, on which high-quality Pb films can be grown.[19] It should be noted that the nomenclature is inverted and that the Bi $\beta$ phase and the Pb $\alpha$ phase are very similar
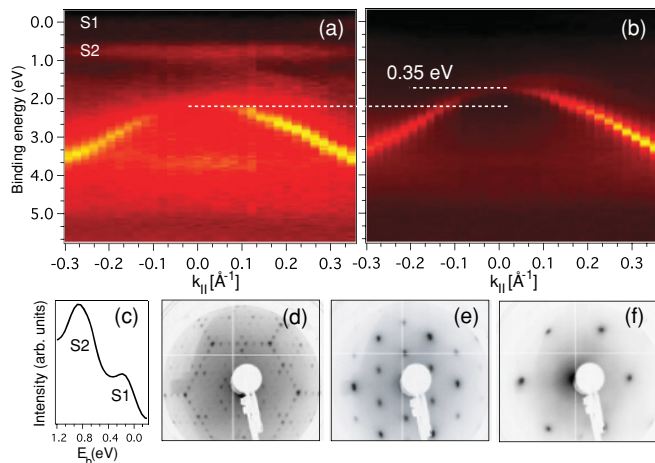
FIG. 1. (Color online) Band dispersion of (a) $n$-Si(111)-($7 \times 7$) and (b) $n$-Si(111)-($\sqrt{3} \times \sqrt{3}$)-Bi($\beta$) along the $\overline{\Gamma M}$ direction. (c) Energy spectrum of $n$-Si(111)-($7 \times 7$) at normal emission. (d–f) LEED patterns from the ($7 \times 7$), Si(111)-($\sqrt{3} \times \sqrt{3}$)-Bi($\beta$) and from the ($1 \times 1$) surface of Pb/Bi/Si(111).

in the sense that both form a trimer-type structure. To avoid confusion we refer to both phases as the dense phase, based on the higher coverage compared to the competing phases.

On these respective $\sqrt{3}$ substrates thin crystalline Pb films were grown by deposition at a rate of $\frac{1}{3}$ ML per minute after cooling down again to below 100 K. For the Pb $\sqrt{3}$ phase it is known that, under these growth conditions, high-quality Pb films that support quantum well states can be grown with monolayer resolution.[4,16,20] One of the findings in this work is that also Pb layers deposited on the Bi interface accommodate well-defined quantum well states.

## III. THE ROLE OF THE METAL-TO-SUBSTRATE INTERFACE

In a first approximation the confinement of the conduction electrons within the metal film can be treated similarly to the well-known one-dimensional particle-in-a-box model. In this model the confinement of a particle by infinite potential barriers leads to discrete energy levels with standing wave solutions having nodes exactly at the boundaries of the box. A more realistic treatment of this problem is to approximate the boundaries by a finite barrier height. In this case the wave function describing the particle will have a certain penetration depth into the barrier specified by a phase shift.[1] The main difference between the two approximations is that, in the case of a finite barrier, the penetration of the wave function will lead to a larger effective width $d$ of the confinement box and therefore to a lower energy of the particle since $E \propto d^{-2}$ (for the same quantum number).

The description of QWSs as standing waves allows application of the so-called phase accumulation model in order to calculate the energies of such electronic states.[21] A standing wave may form when the total accumulated phase $\Phi_T$ is an integer number $n$ of $2\pi$. Here the total phase of the wave can be split into a contribution from the propagation through the overlayer $2dk_z$, when the electron travels back and forth through the medium, and a phase shift upon reflection at

the metal-vacuum interface $\Phi_V$ and at the metal-substrate interface $\Phi_S$:[22]

$$\Phi_T = \Phi_V + \Phi_S + 2d_0 N k_z \overset{!}{=} 2\pi n, \qquad (1)$$

where $d_0$ is the intralayer spacing (Pb; $d_0 = 2.85$ Å) and $N$ denotes the number of monolayers (the thickness of the overlayer is an integral number of $d_0$). In this approach the potentials at the metal-substrate and metal-vacuum interface are simply modeled as a phase shift. The exact nature of the potentials need not necessarily to be known.

While the metal-vacuum interface always produces the same phase shift, the following examples demonstrate the influences of the metal-substrate interface on QWS properties. Ricci *et al.*[23] studied QWS in thin Pb films on three differently terminated Si(111) surfaces, namely, In, Au, and Pb. Although In and Pb induce similar $\sqrt{3}$ reconstructions on Si(111), it was shown that the binding energies differ by $\approx 1$ eV among the two interfaces for the same quantum number $n$ and thickness $d_0 N$. A simultaneous fit of the measured energies using the phase accumulation model together with the interface phase shift according to $\Phi_S(E) = A + B\sqrt{E - E_0}\Theta(E - E_0)$ allows quantification of the influence of the interfaces. Here $E_0$ is the energy of the valence band maximum, $\Theta$ the Heavyside function, and $B$ a constant related to the electronic structure of Si. For Pb the fit yielded $A = 2.21$, and for In $A = -1.70$. The phase shift difference of both interfaces $|\Phi_S^{Pb}(E) - \Phi_S^{In}(E)| \approx \pi$, suggesting that the Pb-interface-induced phase shift $\Phi_S^{Pb}$ is larger than the phase shift induced by the In interface over the entire confinement energy region. As a result, QWSs on the Pb interface are lower in energy, because the effective width of the confinement box is larger. In a similar experiment[5] the influence of the Schottky barrier on the confinement of QWSs was investigated. QWSs with energies $E$ within the band gap of Si(111) cannot couple to any bulk states, thus an electron impinging on the interface will be perfectly reflected. The interface reflectivity is close to 1, resulting in narrow photoemission line shapes. In contrast, electronic states with energies outside the gap, commonly referred to as quantum resonances, give rise to broad peaks due to resonant coupling. By measuring the line width with ARPES as a function of QWS binding energy it is possible to determine the confinement edge $E_0$ and thus the transition from QWS to quantum resonance. For the Pb interface, electronic states with $E_B < 0.55$ eV are truly confined, whereas for the In interface sharp peaks can be observed down to $E_B < 0.58$ eV. These findings are consistent with the determined Schottky barrier, which is 0.62 eV for the Pb and 0.55 eV for the In interface.

To summarize, interfaces of different types of atoms have a significant influence on the phase shift of the wave function at the metal-substrate interface and thus on the electronic properties of QWS. In this work, we show that the interface has also an influence on structural properties of the metallic overlayer and, consequently, on the electronic structure.

## IV. IN-PLANE DISPERSION OF THE QWS

The unusual flat in-plane dispersion of Pb QWSs on Pb-$\sqrt{3}$/Si(111) is still a subject of discussion. Before we present our results and discussion we review some previous

measurements of band dispersions of Pb QWSs on different types of interfaces.

ARPES is a suitable technique to investigate the in-plane dispersion $E(k_\parallel)$ of QWS. The confinement of the states is present in the direction perpendicular to the surface, whereas within the film plane the crystal can be regarded as infinite. Therefore the band structure around the surface Brillouin zone center (SBZC) $\bar{\Gamma}$ ($\vec{k}_\parallel = 0$) is well described by a free electron gas according to $E(k_\parallel) = \frac{\hbar^2}{2m^\star}k_\parallel^2$, with $m^\star$ the effective mass and $\mathbf{k}_\parallel = (k_x, k_y)$ the parallel momentum.

It is known that the dispersion of a band can be attributed to the degree of localization of the state; localized electronic states have less dispersion than delocalized states. In simple systems the degree of localization is related to the degree of overlap between the orbitals of which the state is composed: a small orbital overlap results in a high degree of localization, and vice versa.

An example of a system with almost no interaction between the substrate and the overlayer is given by Pb on graphitized SiC.[24] The dispersion of the QWS is free electron–like, with an effective mass of approximately $m_e$ (free electron mass) around the SBZC even for the low film thickness of 2 ML, where typically, strain due to lattice mismatch with the substrate is expected. Density functional theory (DFT) slab calculations are able to reproduce the measured dispersion by assuming a freestanding Pb slab. In this system the inert graphene layer decouples the influence of the substrate. In contrast, Pb deposited on Pb-$\sqrt{3}$/Si(111) [henceforth Pb/Pb/Si(111)] is an example of a strong influence of the substrate.[16,20] For coverages up to 25 ML the states around the SBZC have unusually high effective masses of up to $m^\star \approx 10\,m_e$, which cannot be modeled with a freestanding film assuming a bulk Pb in-plane lattice constant. Here we show that the Bi interface acts similarly to the graphene layer to decouple the Pb overlayer from the substrate and that the dispersion increases. It will be argued that the strong in-plane localization observed in Pb layers on the Pb-$\sqrt{3}$/Si(111) substrate can be explained by an increased atomic spacing in the direction parallel to the surface induced by the substrate.

## V. RESULTS AND DISCUSSION

Before we discuss the properties of the QWS in Pb films on a Bi-$\sqrt{3}$ interface, we show that this interface is stable against intermixing with the Pb overlayer and that the properties of the QWS do not change significantly on the time scale of days. Each Bi atom of the interface binds covalently with one Si atom of the substrate and with two neighboring Bi atoms, forming the so-called trimer centered at the $T_4$ site.[25] Bonding to the Si atom is stronger than bondings within the trimer, because with increasing substrate temperature the trimer phase can be transferred into the $\alpha$ phase, where only one Bi atom is bound to three Si surface atoms. To investigate possible intermixing we used x-ray photoelectron spectroscopy (XPS) [see Fig. 2(a)] to map the 5$d$ core levels of Bi and Pb.

The red (gray) spectrum corresponds to Bi-$\sqrt{3}$/Si(111), and the black spectrum to 9 ML of Pb on this substrate. The 5$d_{3/2}$ and 5$d_{5/2}$ core levels of Pb and Bi are easily identified and labeled accordingly in Fig. 2(a). The intensities of the Bi core levels are drastically reduced after Pb deposition, which is the
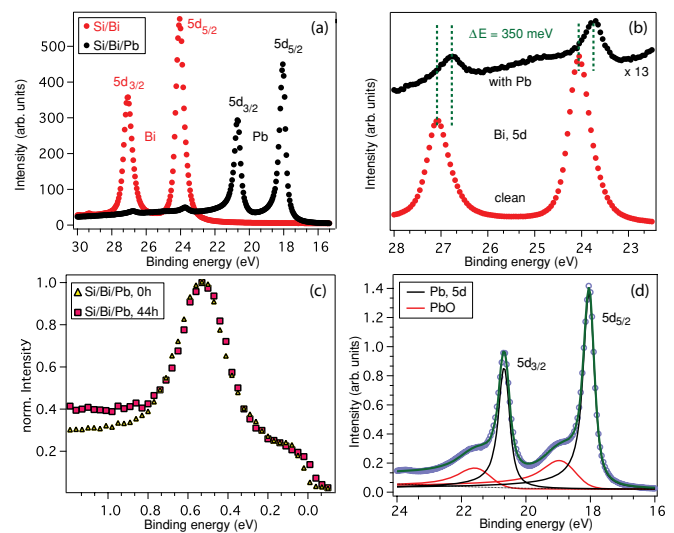


FIG. 2. (Color online) (a) Photoemission of Pb and Bi 5$d$ core levels from Bi-$\sqrt{3}$/Si(111) (red/gray) and of 9-ML Pb/Bi/Si(111) (black). Both heavy metals ($Z_{Pb} = 82$, $Z_{Bi} = 83$) show strong spin-orbit split $d$ states. (b) Core levels of Bi before (red/gray circles) and after Pb deposition (black circles). The Pb overlayer induces a chemical shift by 350 meV toward a lower binding energy. Curves are shifted on the vertical scale for clarity. (c) Spectrum of a QWS shortly after preparation (triangles) and after 44 h (squares). (d) 5$d$ core levels of Pb 24 h after preparation fitted with clean and oxidized Pb components.

first indication that no intermixing occurs at the interface. The remaining Bi intensity is either due to the fact that the Pb layer is not fully closed, and small regions with the bare substrate remain visible, or due to electrons emitted from Bi atoms at the interface. To quantify what Pb thickness would be required for the second scenario, the spectrum after Pb deposition was further analyzed according to Ref. 26, with the Bi interface taken as a 1-ML substrate and the Pb overlayer as a thin film:

$$\frac{I_{Pb}\sigma_{Bi}N^0_{Bi}}{I_{Bi}\sigma_{Pb}N^0_{Pb}} = \frac{1 - \exp\frac{-d_{Pb}}{\lambda_{Pb}}}{\exp\frac{-d_{Pb}}{\lambda_{Pb}} - \exp\frac{-d_{Bi}}{\lambda_{Pb}}}. \qquad (2)$$

Here $I_{Pb}$ and $I_{Bi}$ are the measured intensities, $\sigma$ is the photoionization cross section,[27] for Pb $\sigma_{Pb} = 21.55$ Mb and for Bi $\sigma_{Bi} = 28.03$ Mb, $N$ is the surface atomic density with $N^0_{Pb} = 9.43 \times 10^{14}$ atoms/cm$^2$ and $N^0_{Bi} = 7.83 \times 10^{14}$ atoms/cm$^2$. $d_{Pb}$ and $d_{Bi}$ are the thicknesses of the Pb overlayers and of the Bi layer. $\lambda_{Pb} = 5$ Å is the mean free path of the photoelectrons in the Pb layers. From Eq. (2) we obtain a thickness $d_{Pb} = 18$ Å, which corresponds to 6.1 ML of Pb. From the analysis of the binding energy of the QWS, which provides an intrinsic thickness calibration, we obtain a thickness of 9 ML. In the case of intermixing the ratio of the 5$d$ core-level signals of Pb and Bi would be $I_{Pb} : I_{Bi} = 6 : 1$ for the same amount of Bi in a 9-ML Pb film and, thus, significantly lower than the measured ratio of 56 : 1. We therefore conclude that the Bi interface is stable against intermixing with Pb at the low temperatures under investigation. This result is not suprising since the bonding of the Bi to the Si substrate lowers the surface energy by filling dangling bonds. Although the Bi does not intermix with the Pb, its chemical environment is altered due to the Pb layer on

top. As shown in Fig. 2(b) this results in a shift of the Bi core levels by about 350 meV to lower binding energies.

A further advantage of the investigated ultrathin films is their stability over time. Figure 2(c) shows energy distribution curves (EDCs) of a QWS shortly after preparation (triangles) and after 44 h (squares) of exposure to the residual gas in the ultrahigh vacuum chamber. The $5d$ core levels of Pb [see Fig. 2(d)] show an additional shoulder after 24 h of measurement, which can be attributed to oxidation of the Pb top layer. However, the peak width and the binding energy of the QWS are not affected by this oxidation and remain constant over time. The only quantity that changes is the peak-to-background ratio, which decreases from $1:0.3$ to $1:0.4$ presumably due to an increased number of adsorbates on the surface. This temporal stability of the system is advantageous as it allows performance of long-time measurements, but it also indicates that QWSs survive significant contamination as long as the sample is kept at a low temperature. One would expect a change in the metal-to-vacuum phase shift, when the topmost layer becomes oxidized, which in turn should influence the binding energy of the QWS. However, Peng *et al.* have studied temperature-dependent oxidation of the Pb(111) surface with STM[28] and found that at low temperatures ($\approx 80$ K) and low coverage ($<6$ L), only small oxide clusters form. These clusters serve as point defects, resulting in an increase in the background without a significant change in the confinement of the QWS. Oxidation processes may have an influence on $\Phi_V$ at higher coverages, when a closed oxide layer forms.[29]

Having established the temporal stability of the interface and Pb layers, we now turn to the electronic structure of the quantum well states. Figures 3(a)–3(c) show the in-plane dispersions of QWSs for Pb film thicknesses of 10, 17, and 19 ML grown on a Bi interface measured along the high-symmetry direction $\overline{M}$-$\overline{\Gamma}$-$\overline{M}$ of the $(1 \times 1)$ SBZ. In contrast to Pb films grown on the Pb-$\sqrt{3}$ interface, as shown in Fig. 3(d), we do not observe states with an effective mass larger than 4 $m_e$. The effective mass was determined quantitatively by taking EDCs at momentum steps of $0.035$ Å$^{-1}$ for a total range of $\overline{\Gamma} \pm 0.3$ Å$^{-1}$ and fitting them with Voigt functions after subtracting a linear background contribution. From these fits one obtains the QWS energy versus the in-plane momentum, which is finally fitted assuming a parabolic dispersion to determine $m^\star$.

It should be pointed out that all measured QWS bands presented in this work are derived from $6p$ orbitals, because the binding energies lie above the Pb $sp$ symmetry band gap in the $\overline{\Gamma}$-$\overline{L}$ direction, which expands from 4 to 8 eV in binding energy.[30] Below this gap the QWSs are $6sp_z$ derived. The electronic states described by a parabolic dispersion around the SBZC have a $6p_z$ orbital character and the downward-dispersing bands at $k_{||} > 0.4$ Å$^{-1}$ have a $6p_{xy}$ character.[24]

It is remarkable that, independent of the Pb layer thickness, all measured QWSs exhibit an enhanced in-plane dispersion compared to Pb/Pb/Si(111). The QWS displayed in Fig. 3(a), which is found in a 10-ML-thick film of Pb, has an effective mass of 2.75 $m_e$, and the QWS that arises in 19-ML Pb has an effective mass of 2.09 $m_e$. This trend indicates that the coupling to the substrate is reduced, even for the low coverage, where largest effective masses were reported for Pb/Pb/Si.[16] Figure 3(f) shows the development of the effective mass of
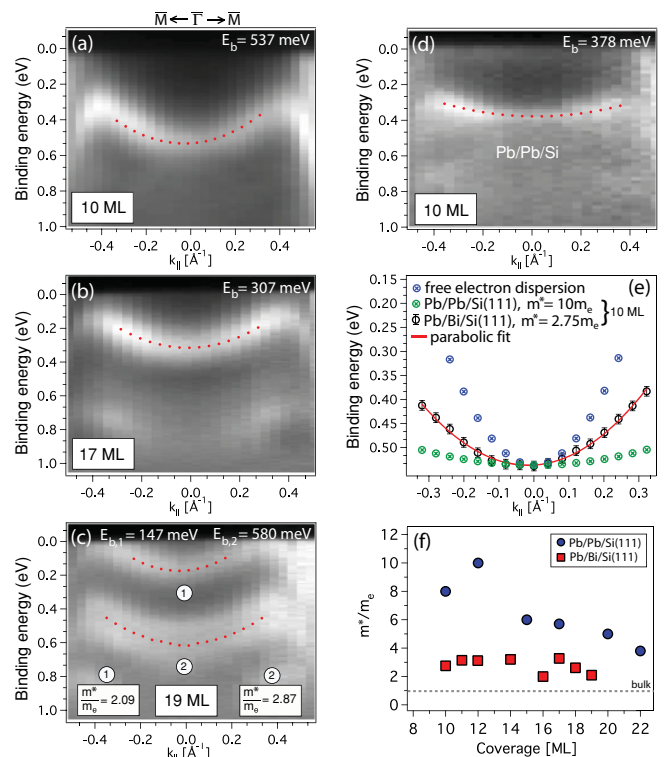


FIG. 3. (Color online) (a–c) Band dispersion of QWSs in 10-, 17-, and 19-ML Pb films on Bi/Si(111). (d) Band dispersion of Pb QWS on Pb/Si(111). (e) Extracted dispersion [(red) circles] from (a) as described in the text. For comparison the free-electron-like dispersion and dispersion of Pb/Pb/Si(111) are included. (f) Squares (red): effective masses of QWS for different thicknesses of Pb deposited on the Bi/Si(111) obtained from the fitting procedure as described in the text. Circles (blue): effective masses of Pb on Pb/Si(111) taken from Ref. 16.

$6p_z$ derived states with an increasing Pb layer thickness for the Pb and the investigated Bi interface. In Pb/Pb/Si(111) the effective mass decreases with thickness, from $m^\star = 10$ $m_e$ at low coverage toward $m^\star = 4$ $m_e$ at 22 ML. With increasing film thickness the effective mass shows a trend toward the bulk limit [$N \to \infty$; dashed (gray) line] of $m^\star = 1.14$ $m_e$.[31] Hence for low coverage the influence of the substrate and interface is most evident, and with increasing thickness this influence becomes smaller.

The substrate may force the atoms in the Pb overlayer into an in-plane lattice constant that coincides more with the lattice structure of the substrate. Thus for low coverage the lattice constant of the overlayer appears to be closer to that of Si than to that of Pb. As a consequence, and because the Pb films grow as close-packed layers in $fcc$ stacking along the [111] direction, an increase in the interatomic distance between nearest-neighbor atoms will decrease the overlap of the $6p_z$ orbitals, as drawn schematically in Figs. 4(a) and 4(b). This in turn leads to more localized states with a flat dispersion. The influence of the substrate becomes less for thicker films, therefore the lattice constant decreases with thickness.

Our interpretation that the degree of orbital overlap influences the band dispersion of Pb QWSs is also supported by DFT calculations, which were performed using the
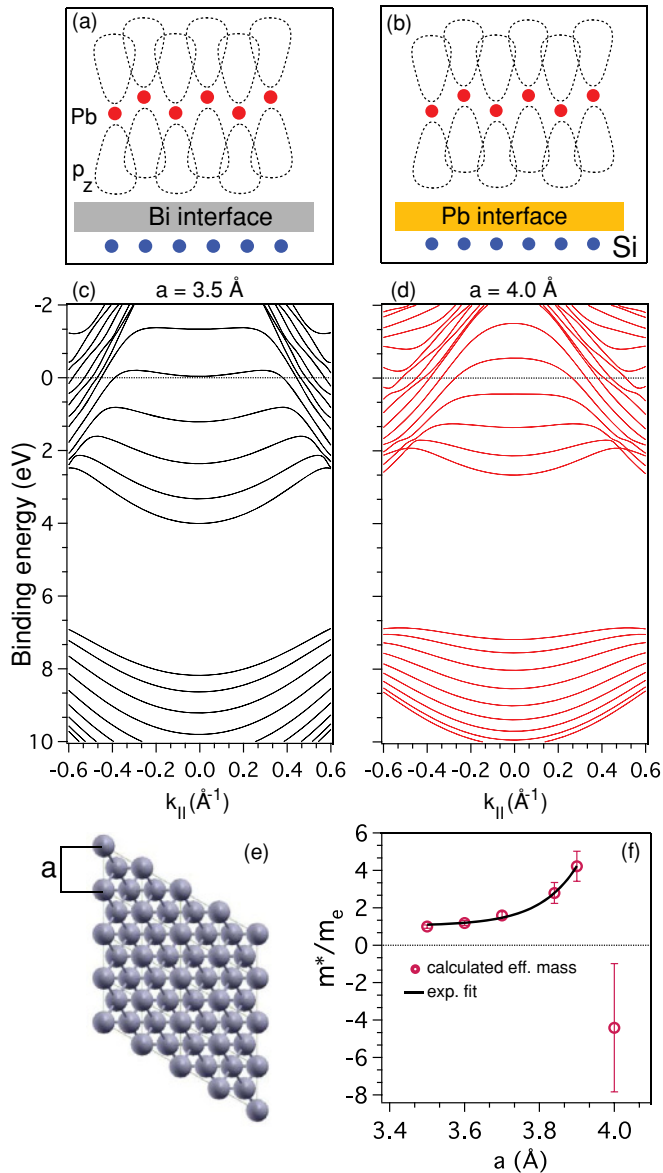
energy range. However, the change of the dispersion of the $6p_z$ states is most significant, which can be assigned to an enhanced influence of the hybridization with the downward dispersing $6p_{xy}$ states. With the increasing in-plane lattice constant, the band width of these bands is reduced, and in the energy range of interest they thus move down in energy and become flatter. The hybridization with the $p_z$ bands, and the associated change from electron-like to hole-like dispersion in these bands, therefore start at a lower $|\mathbf{k}_{\parallel}|$.

In the following analysis we focus on the first band below the Fermi level, as this is the state we measured with ARPES. The effective mass of this band changes from an initial $1.02\, m_e$ to a hole-like dispersion with $m^*$ of $-4.10\, m_e$ when the lattice constant is increased by 0.5 Å. Figure 4(f) shows calculated effective masses for lattice parameters between 3.5 and 4.0 Å, which are fitted for positive values with an exponential function according to $m^*(a[\text{Å}]) = 1.038 + 0.0585 \exp(\frac{a-3.5}{0.1})$ in units of the free electron mass. Note that the influence of the lattice parameter on the effective mass is weak up to $a = 3.7$ Å and becomes stronger for higher values. This anomalous dependency of the effective mass on the in-plane lattice constant thus is not only a result of the reduced orbital overlap but also strongly enhanced by the hybridization of the $6p_z$ and $6p_{xy}$ derived bands.

Having confirmed by DFT the influence of the in-plane lattice constant on the band dispersion, we now turn to the measurements of the surface in-plane lattice constants using LEED, which is sensitive to the surface atomic structure and thus allows determination of changes in the in-plane lattice constant of the topmost layers. We have recorded the $(1 \times 1)$ LEED patterns of the Pb surface for different coverages of Pb on Pb-$\sqrt{3}$/Si(111) and for a 10-ML-thick Pb film on Bi-$\sqrt{3}$/Si(111). A comparison of the $(1,0)$ spots for the 10-ML-thick film grown on the different interfaces indicates that the spots are sharper on the Bi interface than on the Pb interface as shown in the raw data in Figs. 5(a) and 5(b) and the profiles in Fig. 5(c). Sharp LEED spots are found either for perfectly commensurate systems or when the interaction between the substrate and the overlayer is minimal.[24]

For a more quantitative determination of the in-plane lattice constant, the LEED data were analyzed as follows: First, a two-dimensional Gaussian fit as shown in Figs. 5(a) and 5(b) determines the position of each spot and the corresponding $(x, y)$ coordinates on the screen. Second, from these coordinates the distances between all three $\overline{\text{M}}$-$\overline{\Gamma}$-$\overline{\text{M}}$ directions were determined, and, finally, averaged. Although our LEED setup is sensitive to relative changes in the lattice constant, it is not calibrated for the precise determination of absolute values. In the following we therefore use values relative to the atomic spacing found for the lowest thickness of Pb on Pb-$\sqrt{3}$/Si(111). The findings are summarized in Fig. 5(d) as a function of layer thickness. The thinnest Pb layer, 3 ML on the Pb interface has an almost 2% larger lattice constant than the 20-ML Pb film on the same substrate. Using the relation between lattice constant and effective mass obtained from DFT, we can calculate the corresponding lattice constant for the 20-ML-thick Pb film ($m^* = 5\, m_e$), which is 3.921 Å [Fig. 4(f)], and estimate the effective mass for this lattice constant expanded by 2% (3.999 Å). This gives us $m^* = 9.689\, m_e$, which is in very good agreement with what is observed for low coverages. The lattice



FIG. 4. (Color online) (a, b) Simplified picture of $p_z$ orbital overlap at both interfaces. (c) Calculated band dispersion along $\overline{\text{M}}$-$\overline{\Gamma}$-$\overline{\text{M}}$ with an in-plane lattice constant of (c) $a = 3.5$ Å and (d) $a = 4.0$ Å. (e) Top view of the Pb(111) surface and (f) effective masses for different in-plane lattice constants obtained from DFT including an exponential fit as described in the text.

*ab initio* Wien2K simulation package.[32] The generalized gradient approximation of Perdew *et al.*[33] was applied to a repeated slab geometry (8-ML Pb, 15-Å vacuum) with a muffin-tin radius set to $2.5\, a_0$, plane wave cutoff of 7.84 Ry, and integration over the Brillouin zone with $(16 \times 16 \times 1)\, k$ points. Spin-orbit interaction was included in a second self-consistent cycle using pertubation theory with the scalar-relativistic orbitals as basis set. Figures 4(c) and 4(d) show two band dispersions along $\overline{\text{M}}$-$\overline{\Gamma}$-$\overline{\text{M}}$ for the in-plane lattice constants $a = 3.5$ and 4.0 Å as defined in Fig. 4(e).

The increase in the in-plane lattice constant by 0.5 Å affects the entire band dispersion of the system. Both the $6p_z$ derived bands and the $6sp_z$ derived bands below the symmetry band gap of Pb become flatter throughout the whole
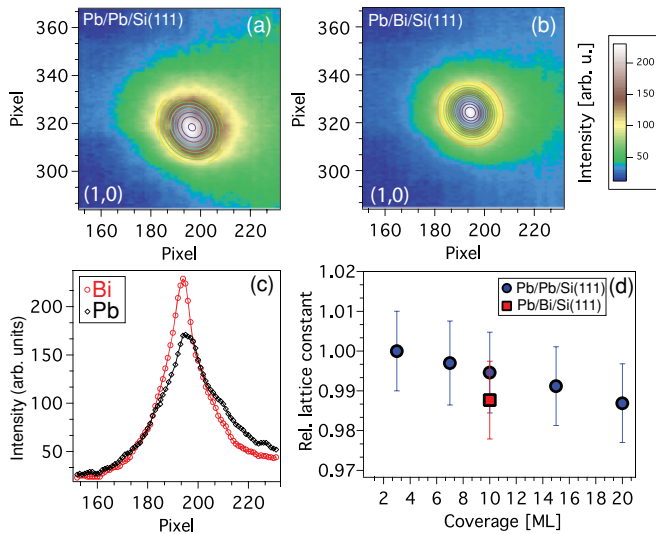
FIG. 5. (Color online) (a, b) (1,0) LEED spot of a Pb/Pb/Si(111) and Pb/Bi/Si(111) surface. (c) Horizontal cut through the maximum of intensity of the (1,0) spot for Bi [open (red) circles] and Pb [filled (black) circles]. (d) Relative lattice constant vs. coverage measured with LEED; (blue) circles represent Pb/Pb/Si(111); (red) square, Pb/Bi/Si(111).

constant of the 10-ML Pb film grown on the Pb-$\sqrt{3}$/Si(111) differs by about 1% from that of the Pb film grown on the Bi interface. Comparison of these effective masses with our fit function leads to a lattice constant difference of almost 3%, which is consistent within our error margins.

These small changes in the in-plane lattice constant may in principle also be observed in surface x-ray diffraction studies, which has a higher resolution than LEED and probes the full layer and not only the topmost layers. In two surface x-ray diffraction studies on this system,[34,35] the exact in-plane lattice distance could unfortunately not be determined exactly, and it was only found that the in-plane spacing is "bulk-like," with a relatively large distribution, which is also reflected in the broad LEED spots shown in Figs. 5(a) and 5(c). In STM measurements a mismatch between the substrate and the overlayer in-plane lattice constants can be resolved through an analysis of the resulting Moiré pattern. From such measurements on Pb-$\sqrt{3}$/Si(111) combined with high-resolution LEED data for low coverages,[36] it was determined that the Pb and Si lattice constants are not the same. Here again, the exact in-plane lattice spacing of the Pb film cannot be determined because the measured corrugation is a convolution of the Moiré pattern, the changes in the local density of states, and the surface relaxation. Although the determination of the exact in-plane lattice constant has proven very difficult, the relative changes in the in-plane lattice constant obtained from our LEED analysis correlate well with the measured changes in effective mass, as supported by our DFT results.

Upton *et al.* have attempted to explain the unusually high effective mass in Pb/Pb/Si(111) in terms of an avoided crossing of $p_z$ derived states and valence states of Si(111) and the rapid oscillations of the phase shift in this energy region.[15] QWSs with energies close to the confinement edge $E_0$ of the substrate will feel a repulsive force, which tends to lower the binding energy and so to prevent a band crossing. Figure 6(a) shows
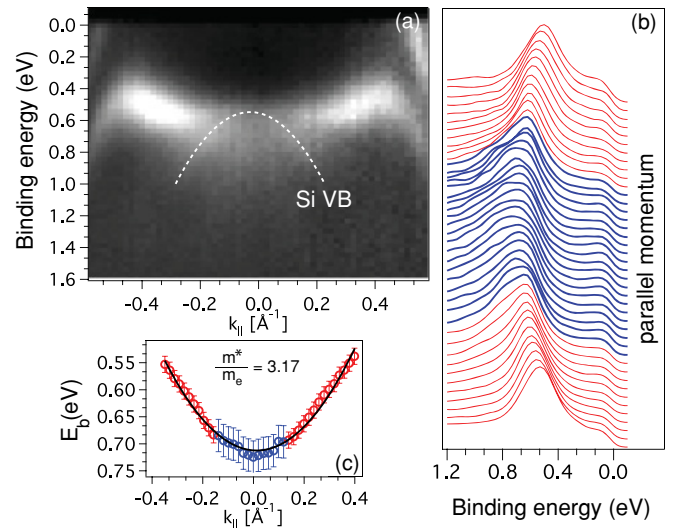


FIG. 6. (Color online) (a) Band dispersion of 12-ML Pb deposited on top of Bi/Si(111). (b) Normalized energy distribution curves for in-plane momenta $k_\parallel = 0 \pm 0.4$ Å$^{-1}$. Blue spectra represent quantum resonances; red (gray) spectra, fully confined QWSs. (c) Parabolic fit including the quantum resonances.

the band dispersion of a 12-ML Pb film grown on the Bi-$\sqrt{3}$ interface with a binding energy of $E_B = 690$ meV at the zone center and with an effective mass of $m^\star = 3.17\,m_e$.

The parabolic band dispersion of the Pb film intersects with the VB of Si around an in-plane momentum of $k_\parallel = (0 \pm 0.2)$ Å$^{-1}$ and becomes less pronounced in this region. Electronic states farther away from the VB are not affected. Interaction of film states with the VB of the substrate was also reported for Al/Si(111)[37] and Ag/Ge(111)[38] and explained in terms of hybridization of the film and valence states of the substrate. States within the specific momentum range around $\overline{\Gamma}$ are quantum resonances, because they are not confined within the absolute band gap of Si(111). The hybridization leads to a lower intensity and to a larger peak width because the reflectivity of the interface is no longer equal to one. Figure 6(b) shows EDCs taken from $k_\parallel = -0.4$ to $+0.4$ Å$^{-1}$ and normalized to the maximum intensity. Red (light-gray) EDCs represent truly confined states (QWSs) with narrow line widths; blue (dark-gray) EDCs, quantum resonances. Also, for the Bi reconstructed interface a clear hybridization between the QWS and the Si VB is thus observed. However, the effective mass is still significantly lower compared to that for QWSs on Pb-$\sqrt{3}$/Si(111). Therefore the high effective mass for Pb/Pb/Si(111) cannot be explained by the influence of the Si VB alone. The increase in the effective mass actually occurs in an energy and momentum space that is farther away from the Si valence band and closer to the $6p_{xy}$ derived states. Thus the unusual effective mass in Pb/Pb/Si(111) arises from the structural and electronic properties of the Pb overlayer and can be reduced by replacing the Pb with a Bi interface.

## VI. SUMMARY

The influence of the Bi interface on the in-plane dispersion of $6p_z$ derived QWSs has been studied with ARPES and LEED experiments and DFT calculations. In contrast to

Pb/Pb/Si(111), we find (i) no effective masses larger than 4 $m_e$ and (ii) no significant dependence of the effective mass on the layer thickness. Compared to Pb/Pb/Si(111), the dispersion of $6p_z$ derived states in Pb/Bi/Si(111) is enhanced. With LEED we confirmed that in Pb/Pb/Si(111) the in-plane lattice constant of the ultrathin film decreases with coverage in a manner similar to that for the effective mass. This is fully consistent with our DFT calculations and the corresponding picture of orbital overlap; the reduced overlap of $6p_z$ orbitals reduces the dispersion; simultaneously the band width of the $6p_{xy}$ derived states is reduced. Together, these effects alter the hybridization between $6p_z$ and $6p_{xy}$ derived bands and cause the change from electron-like to hole-like dispersion to shift to a lower $|\mathbf{k}_\parallel|$. Furthermore, the in-plane lattice constant of

a Pb film on a Bi reconstructed interface is smaller compared to a film of similar coverage on a Pb reconstructed interface, which is also reflected in the effective mass. These findings let us conclude that the Bi interface acts as a decoupling layer between the Pb and the Si, in the sense that the influence of the substrate on lateral atomic positions of the Pb overlayer is reduced.

*bartosz.slomski@psi.ch

[1] T. -C. Chiang, Surf. Sci. Rep. **39**, 181 (2000).

[2] F. K. Schulte, Surf. Sci. **55**, 427 (1976).

[3] J. H. Dil, B. Hülsen, T. U. Kampen, P. Kratzer, and K. Horn, J. Phys. Condens. Matter **22**, 135008 (2010).

[4] V. Yeh, L. Berbil-Bautista, C. Z. Wang, K. M. Ho, and M. C. Tringides, Phys. Rev. Lett. **85**, 5158 (2000).

[5] D. A. Ricci, T. Miller, and T.-C. Chiang, Phys. Rev. Lett. **93**, 136801 (2004).

[6] D. R. Heslinga, H. H. Weitering, D. P. van der Werf, T. M. Klapwijk, and T. Hibma, Phys. Rev. Lett. **64**, 1589 (1990).

[7] K. Budde, E. Abram, V. Yeh, and M. C. Tringides, Phys. Rev. B **61**, R10602 (2000).

[8] G. Yang *et al.*, Science **306**, 1915 (2004).

[9] C. Brun, I.-P. Hong, F. Patthey, I. Yu. Sklyadneva, R. Heid, P. M. Echenique, K. P. Bohnen, E. V. Chulkov, and W.-D. Schneider, Phys. Rev. Lett. **102**, 207002 (2009).

[10] E. Daejin, S. Qin, M.-Y. Chou, and C. K. Shih, Phys. Rev. Lett. **96**, 027005 (2006).

[11] P. S. Kirchmann, M. Wolf, J. H. Dil, K. Horn, and U. Bovensiepen, Phys. Rev. B **76**, 075406 (2007).

[12] P. S. Kirchmann and U. Bovensiepen, Phys. Rev. B **78**, 035437 (2008).

[13] J. H. Dil, F. Meier, J. Lobo-Checa, L. Patthey, G. Bihlmayer, and J. Osterwalder, Phys. Rev. Lett. **101**, 266802 (2008).

[14] A. Mans, J. H. Dil, A. R. H. F. Ettema, and H. H. Weitering, Phys. Rev. B **66**, 195410 (2002).

[15] M. H. Upton, T. Miller, and T.-C. Chiang, Phys. Rev. B **71**, 033403 (2005).

[16] J. H. Dil, J. W. Kim, Th. Kampen, K. Horn, and A. R. H. F. Ettema, Phys. Rev. B **73**, 161308 (2006).

[17] M. Hoesch, Ph.D. thesis, University of Zurich, 2002.

[18] K. J. Wan, T. Guo, W. K. Ford, and J. C. Hermanson, Phys. Rev. B **44**, 3471 (1991).

[19] M. Hupalo, V. Yeh, L. Berbil-Bautista, S. Kremmer, E. Abram, and M. C. Tringides, Phys. Rev. B **64**, 155307 (2001).

[20] M. H. Upton, C. M. Wei, M. Y. Chou, T. Miller, and T.-C. Chiang, Phys. Rev. Lett. **93**, 026802 (2004).

[21] N. V. Smith, Phys. Rev. B **32**, 3549 (1985).

[22] P. M. Echenique and J. B. Pendry, J. Phys. C **11**, 2065 (1978).

[23] D. A. Ricci, Y. Liu, T. Miller, and T.-C. Chiang, Phys. Rev. B **79**, 195433 (2009).

[24] J. H. Dil, T. U. Kampen, B. Hülsen, T. Seyller, and K. Horn, Phys. Rev. B **75**, 161401 (2007).

[25] C. Cheng and K. Kunc, Phys. Rev. B **56**, 10283 (1997).

[26] G. Ertl and J. Küppers, *Low Energy Electrons and Surface Chemistry*, 2nd ed. (VCH, Weinheim, 1985).

[27] J. J. Yeh and I. Lindau, *Atomic Calculation of Photoionization Cross-Sections and Asymmetry Parameters* (Gordon and Breach Science, Langhorne, PA, 1993).

[28] J. Peng, L.-L. Wang, Y.-X. Ning, Y. Qi, X.-C. Ma, J.-F. Jia, and Q.-K. Xue, Chin. Phys. Lett. **26**, 016803 (2009).

[29] Z. Hu, Y. Yang, B. Sun, X. Shao, W. Wang, and P. Zhang, J. Chem. Phys. **132**, 024703 (2010).

[30] K. Horn, B. Reihl, A. Zartner, D. E. Eastman, K. Hermann, and J. Noffke, Phys. Rev. B **30**, 1711 (1984).

[31] B. J. Hinch, C. Koziol, J. P. Toennies, and G. Zhang, Europhys. Lett. **10**, 341 (1989).

[32] K.arlheinz Schwarz and P. Blaha, Comput. Mater. Sci. **28**, 259 (2003).

[33] J. P. Perdew, K. Burke, and M. Ernzerhof, Phys. Rev. Lett. **77**, 3865 (1996).

[34] P. Czoschke, H. Hawoong, L. Basile, and T.-C. Chiang, Phys. Rev. B **72**, 035305 (2005).

[35] P. Czoschke, H. Hawoong, L. Basile, and T.-C. Chiang, Phys. Rev. B **72**, 075402 (2005).

[36] M. Hupalo, V. Yeh, T. L. Chan, C. Z. Wang, K. M. Ho, and M. C. Tringides, Phys. Rev. B **71**, 193408 (2005).

[37] L. Aballe, C. Rogero, P. Kratzer, S. Gokhale, and K. Horn, Phys. Rev. Lett. **87**, 156801 (2001).

[38] P. Moras, D. Topwal, P. M. Sheverdyaeva, L. Ferrari, J. Fujii, G. Bihlmayer, S. Blügel, and C. Carbone, Phys. Rev. B **80**, 205418 (2009).